Noname manuscript No.
(will be inserted by the editor)

Extension of Sea Surface Temperature Unpredictability

Marat Akhmet · Mehmet Onur Fen · Ejaily Milad Alejaily

Received: date / Accepted: date

Abstract It was Vallis [37] who revealed unpredictability in El Niño-Southern Oscillation (ENSO) by reducing his model to the Lorenz equations. We discuss the unpredictability for sea surface temperature (SST) as an extendable phenomenon through coupled Vallis ENSO models and advection equations by using theoretical as well as numerical analyses. To perform theoretical research, we apply our recent results on replication of chaos and unpredictable solutions of differential equations, while for numerical analysis, we combine results on unpredictable solutions with numerical analysis of chaos in the advection equation.

Keywords Sea surface temperature · Unpredictability extension · El Niño-Southern Oscillation · Vallis model · Advection equation

Acknowledgment The authors wish to express their sincere gratitude to the referees for the helpful criticism and valuable suggestions, which helped significantly improve the paper.

The third author is supported by a scholarship from the Ministry of Education, Libya.

1 Introduction and Preliminaries

In meteorology and climate science, SST is considered as a very important factor in ocean-atmosphere interaction, where it plays a basic role in determining the magnitude and direction of the current velocity, as well as the

Marat Akhmet
Department of Mathematics, Middle East Technical University, 06800 Ankara, Turkey
Tel.: +90 312 210 5355
Fax: +90 312 210 2972
E-mail: marat@metu.edu.tr

Mehmet Onur Fen
Department of Mathematics, TED University, 06420 Ankara, Turkey

Ejaily Milad Alejaily
Department of Mathematics, Middle East Technical University, 06800 Ankara, Turkey

ocean surface wind speed. It is difficult to give a precise definition of SST due to the complexity of the heat transfer operations in the mixed layer of upper ocean. In general, however, it can be defined as the bulk temperature of the oceanic mixed layer with a depth varies from $1\,m$ to $20\,m$ depending on the measurement method used [7]. The importance of SST stems from the fact that the world's oceans cover over 70 % of the whole surface of the globe. This large contact area gives way to an active ocean-atmosphere interaction and sometimes becomes a fertile place for complex feedbacks between the ocean and atmosphere that drive an irregular climate change.

The most important example of the interactions and feedbacks between the ocean and the atmosphere is El Niño and Southern Oscillation which is defined as a global coupled ocean-atmosphere phenomenon occurs irregularly in the Pacific Ocean about every 2 to 7 years [35]. Besides the ENSO, there are several other atmospheric patterns that occur in different regions of the Earth. These phenomena are interacting in very complicated ways. The Indian Ocean Dipole (IOD), for instant, is the most similar atmosphere-ocean coupled phenomenon to ENSO. It occurs in the tropical Indian Ocean, and it is sometimes called the Indian Niño. A symmetrical correlation have been observed between the IOD and ENSO mechanisms. Indeed, SST data shows that the Indian Ocean warming appears as a near mirror image of ENSO in the Pacific [12]. In addition, the IOD is likely to have a link with ENSO events, where the positive (negative) phase of IOD often occurs during El Niño (La Nina) phase of ENSO [15,39]. Luo et al. [25] investigated the ENSO-IOD interactions, and they suggest that IOD may significantly enhance ENSO and its onset forecast, and vice versa. Several other researchers like Behera et al. [9] and Roxy et al. [29] studied the relationship and interaction between ENSO and IOD. It should be noted here that (as in all these studies) the SST considered as the major variable, indicator and index for these events.

There are different hypotheses for the source of chaos in ENSO. According to Neelin and Latif [27], deterministic chaos within the nonlinear dynamics of coupled system, uncoupled atmospheric weather noise and secular variation in the climatic state are the possible source of ENSO irregularity. Tziperman et al. [36] concluded that the chaotic behavior of ENSO is caused by the irregular jumping of the ocean-atmosphere system among different nonlinear resonances. Several studies like [8,28] support this assumption and attributed the irregularity and the unpredictability of ENSO to influence of stochastic forcing generated by weather noise. Other studies like [40,26] infer that ENSO is intrinsically chaotic, which means that the irregularity and the loss of predictability are independent of the chaotic nature of weather.

Practically, investigating chaos in ENSO needs long time-series of data, which make the task quite difficult experimentally. Vallis [37], developed a conceptual model of ENSO and suggested that the ENSO oscillation exhibits a chaotic behavior. Vallis used finite difference formulation to reduce two dimensional versions of advection and continuity equations to a set of ordinary differential equations. In addition, he assumed that the zonal current is driven by the surface wind, which is in turn proportional to the temperature difference

across the ocean. The model is described by the set of equations

$$\begin{aligned}\frac{du}{dt} &= \beta\,(T_e - T_w) - \lambda\,(u - u^*),\\ \frac{dT_w}{dt} &= \frac{u}{2\Delta x}\,(\bar{T} - T_e) - \alpha\,(T_w - T^*),\\ \frac{dT_e}{dt} &= \frac{u}{2\Delta x}\,(T_w - \bar{T}) - \alpha\,(T_e - T^*),\end{aligned} \tag{1}$$

where u represents the zonal velocity, T_w and T_e are the SST in the eastern and western ocean respectively, $\bar{T}$ is the deep ocean temperature, T^* is the steady state temperature of ocean, u^* represents the effect of the mean trade winds, Δx is the width of the ocean basin, and α, β and λ are constants.

By nondimensionalizing Eqs. 1 and forming the sum and difference of the two temperature equations, one can see that these equations have the same structure as the Lorenz system. Vallis utilized the fact that the Lorenz system, with specific parameters, is intrinsically chaotic, and showed that a chaotic behavior of the sum and difference of the west and east SST can be obtained.

The temporal and spatial evolution of the SST is governed by a first order quasi-linear partial differential equation, the advection equation. If we denote the SST by T, the temperature advection equation of mixed layer of fixed depth can be written in the form [38, 23]

$$\frac{\partial T}{\partial t} + u\frac{\partial T}{\partial x} + v\frac{\partial T}{\partial y} + w\frac{\partial T}{\partial z} = f(t, x, y, z, T), \tag{2}$$

where u, v, w are the zonal, meridional and vertical components of current velocity, respectively. These velocities theoretically must satisfy the continuity equation

$$\frac{\partial}{\partial x}(\rho u) + \frac{\partial}{\partial y}(\rho v) + \frac{\partial}{\partial z}(\rho w) = -\frac{\partial \rho}{\partial t}, \tag{3}$$

where ρ is the seawater density.

The inhomogeneous (forcing) term f on the right-hand side of Eq. 2 consists of the shortwave flux, the evaporative heat flux, the combined long-wave back-radiation and sensible heat flux and heat flux due to vertical mixing [21]. This term can be described by [18, 34, 20]

$$f \approx \frac{1}{h\rho\, C_p}\,\frac{\partial q}{\partial z} + D, \tag{4}$$

where h is the mixed layer depth, C_p is the heat capacity of seawater, q is radiative and diffusive heat flux, and D is the thermal damping (the numerical diffusion operator).

The spatial and temporal domain of Eq. 2 depend on the region and the nature of the phenomenon under study. For studying ENSO or IOD, for instance, there are various regions for monitoring SST. NINO3.4 is one of the

most commonly used indices for ENSO. Dipole Mode Index (DMI) is usually used for IOD, and it depends on the difference in average SST anomalies between the western 50°E–70°E, 10°N–10°S and the eastern 90°E–110°E, 0°–10°S boxes [30]. The mixed layer depth h varies with season and depends on the vertical heat flux through the upper layers of the ocean. The average of mixed layer depth is about 30 m [24]. Different studies of ocean-atmosphere coupled models considered different regions of various sizes. Zebiak and Cane [40], for example, developed a model of ENSO. They considered a rectangular model extending from 124°E to 80°W and 29°N to 29°S, with constant mixed layer depth of 50 m and 90 years simulation.

From the above we find that the domain of Eq. 2 depends on the purpose of the study. To study ENSO, for instance, we would cover a big region of pacific ocean basin, and if we choose the origin of coordinates to be at 160°E on the Equator, we can write the domain of (2) as follows

$$t \geq 0, \quad 0 \leq x \leq 9000\,\text{km}, \quad -3000\,\text{km} \leq y \leq 3000\,\text{km}, \quad -100\,\text{m} \leq z \leq 0.$$

The inhomogeneous term in Eq. 2, which includes mixing processes of heat transfer, plays the main role for chaotic dynamics. In addition to this term, a chaotic behavior in ocean current velocity terms may also produce an unpredictable behavior in SST. These causes of unpredictability are proved analytically and numerically by perturbing these terms by unpredictable functions. In this study we treat Eq. 2 mathematically without paying attention to the dimensions of the physical quantities. The important thing to us is the possibility of presence of chaos in this advection equation endogenously or be acquired from other equation or system. The advection equation, in addition to the Vallis model, will be used to demonstrate the extension of unpredictability through the ocean.

There are different types and definitions of chaos. Devaney [14] and Li-Yorke [22] chaos are the most frequently used types, which are characterized by transitivity, sensitivity, frequent separation and proximality. Another common type is the period-doubling cascade, which is a sort of route to chaos through local bifurcation [16,32,31]. In the papers [3,2], Poincaré chaos was developed by introducing the theory of unpredictable point and unpredictable function, which are built on the concepts of Poisson stable point and function. We define unpredictable point as follows. Let (X, d) be a metric space and $\pi : \mathbb{T} \times X \to X$ be a flow on X, where $\mathbb{T}$ refer to either the set of real numbers or the set of integers. We assume that the triple (π, X, d) defines a dynamical system.

Definition 1 *[3] A point $p \in X$ and the trajectory through it are unpredictable if there exist a positive number ϵ (the unpredictability constant) and sequences $\{t_n\}$, $\{\tau_n\}$ both of which diverge to infinity such that $\lim_{n\to\infty} \pi(t_n, p) = p$ and $d[\pi(t_n + \tau_n, p), \pi(\tau_n, p)] \geq \epsilon$ for each $n \in \mathbb{N}$.*

Definition 1 describes unpredictability as individual sensitivity for a motion, i.e., it is formulated for a single trajectory. The Poincaré chaos is distinguished

by Poisson stable motions instead of periodic ones. Existence of infinitely many unpredictable Poisson stable trajectories that lie in a compact set meet all requirements of chaos. Based on this, chaos can be appeared in the dynamics on the quasi-minimal set which is the closure of a Poisson stable trajectory. Therefore, the Poincaré chaos is referred to as the dynamics on the quasi-minimal set of trajectory initiated from unpredictable point.

The definition of an unpredictable function is as follows.

Definition 2 *[5] A uniformly continuous and bounded function $\varphi : \mathbb{R} \to \mathbb{R}^m$ is unpredictable if there exist positive numbers ϵ, δ and sequences $\{t_n\}$, $\{\tau_n\}$ both of which diverge to infinity such that $\|\varphi(t + t_n) - \varphi(t)\| \to 0$ as $n \to \infty$ uniformly on compact subsets of $\mathbb{R}$, and $\|\varphi(t + t_n) - \varphi(t)\| \geq \epsilon$ for each $t \in [\tau_n - \delta, \tau_n + \delta]$ and $n \in \mathbb{N}$.*

To determine unpredictable functions, we apply the uniform convergence topology on compact subsets of the real axis. This topology allows us to construct Bebutov dynamical system on the set of the bounded functions [4,33]. Consequently, the unpredictable functions imply presence of the Poincaré chaos.

2 Unpredictable Solution of the Advection Equation

In this section we study the presence of Poincaré chaos in the dynamics of Eq. 2. We expect that the behavior of the solutions of (2) depends on the function f and the current velocity components u, v, w, which are used in the equation. From Eq. 4, we see that the forcing term f depends mainly on the heat fluxes between the sea surface and atmosphere which is governed by SST, air temperature and wind speed, as well as between layers of sea which is caused by sea temperature gradient and vertical (entrainment) velocity. Therefore, this forcing term can be a natural source of noise and irregularity. Ocean currents are mainly driven by wind forces, as well as temperature and salinity differences [13]. Thence again we can deduce that the irregular fluctuations of wind may be reflected in the behavior of SST.

To demonstrate the role of the function f in the dynamics of Eq. 2, let us take into account the equation

$$\frac{\partial T}{\partial t} + u\frac{\partial T}{\partial x} + v\frac{\partial T}{\partial y} + w\frac{\partial T}{\partial z} = -0.7\,T + 0.3\,w_1\,T + 5\,\sin(xt), \tag{5}$$

where the current velocity components are defined by $u = \sin(\frac{x}{2}) + \sin(t) + 3$, $v = -0.02$, and $w = -\frac{1}{2}\cos(\frac{x}{2})z$.

Figure 1 represents the solution of (5) corresponding to the initial data $T(0, 0, 0, 0) = 0.5$. It is seen in Fig. 1 that the solution of Eq. 5 has an irregular oscillating behavior, whereas in the absence of the term $5\sin(xt)$ in the function f, the solution approaches the steady state. Even though the behavior of this numerical solution depends on the step size of the numerical scheme used, this situation leads us to consider that the forcing term f has a dominant role in the behavior of SST.

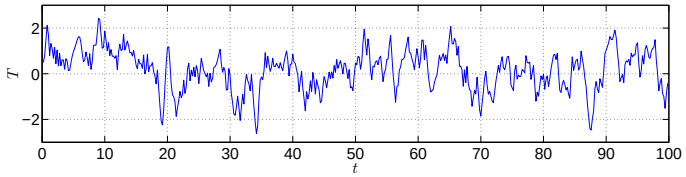

Fig. 1 The solution of Eq. 5 with the initial condition $T(0,0,0,0) = 0.5$. The figure shows that the forcing term f has a significant role in the dynamics of (2).

To investigate the existence of an unpredictable solution in the dynamics of Eq. 2 theoretically, let us apply the method of characteristics. If we parametrize the characteristics by the variable t and suppose that the initial condition is given by $T(t_0, x, y, z) = \Phi(x, y, z)$, where t_0 is the initial time, then we obtain the system

$$\begin{aligned} \frac{dx}{dt} &= u(t, x, y, z, T), \\ \frac{dy}{dt} &= v(t, x, y, z, T), \\ \frac{dz}{dt} &= w(t, x, y, z, T), \\ \frac{dT}{dt} &= f(t, x, y, z, T), \end{aligned} \tag{6}$$

with the initial conditions

$$x(t_0) = x_0, \quad y(t_0) = y_0, \quad z(t_0) = z_0, \quad T(t_0, x_0, y_0, z_0) = \Phi(x_0, y_0, z_0).$$

In system (6), we assume that u, v, w, and f are functions of x, y, z, t, and T, and they have the forms

$$\begin{aligned} u &= a_1\, x + a_2\, y + a_3\, z + a_4\, T + U(x, y, z, T), \\ v &= b_1\, x + b_2\, y + b_3\, z + b_4\, T + V(x, y, z, T), \\ w &= c_1\, x + c_2\, y + c_3\, z + c_4\, T + W(x, y, z, T), \\ f &= d_1\, x + d_2\, y + d_3\, z + d_4\, T + F(x, y, z, T), \end{aligned} \tag{7}$$

where a_i, b_i, c_i, d_i, $i = 1, 2, 3, 4$, are real constants and the functions U, V, W, F are continuous in all their arguments. System (6) can be expressed in the form

$$X'(t) = AX(t) + Q(t), \tag{8}$$

in which

$$X(t) = \begin{bmatrix} x \\ y \\ z \\ T \end{bmatrix}, \qquad A = \begin{bmatrix} a_1 & a_2 & a_3 & a_4 \\ b_1 & b_2 & b_3 & b_4 \\ c_1 & c_2 & c_3 & c_4 \\ d_1 & d_2 & d_3 & d_4 \end{bmatrix}, \qquad Q = \begin{bmatrix} U \\ V \\ W \\ F \end{bmatrix}. \tag{9}$$

The following theorem is needed to verify the existence of Poincaré chaos in the dynamics of Eq. 2.

Theorem 1 *[2] Consider the system of ordinary differential equations*

$$X'(t) = A\,X(t) + G(X(t)) + H(t), \tag{10}$$

where the $n \times n$ constant matrix A has eigenvalues all with negative real parts, the function $G : \mathbb{R}^n \to \mathbb{R}^n$ is Lipschitzian with a sufficiently small Lipschitz constant, and $H : \mathbb{R} \to \mathbb{R}^n$ is a uniformly continuous and bounded function. If the function $H(t)$ is unpredictable, then system (10) possesses a unique uniformly exponentially stable unpredictable solution, which is uniformly continuous and bounded on the real axis.

In the remaining parts of the present section, we will discuss the unpredictability when SST is chaotified by external irregularity. For that purpose let us consider the logistic map

$$\eta_{j+1} = 3.91\,\eta_j\,(1 - \eta_j),\ j \in \mathbb{Z}. \tag{11}$$

According to Theorem 4.1 [2], the map (11) is Poincaré chaotic such that it possesses an unpredictable trajectory.

Next, we define a function $\phi(t)$ by

$$\phi(t) = \int_{-\infty}^{t} e^{-2(t-s)}\gamma^*(s)\,ds, \tag{12}$$

where

$$\gamma^*(t) = \begin{cases} 1.5, & \zeta^*_{2j} < t \le \zeta^*_{2j+1}, \quad j \in \mathbb{Z}, \\ 0.3, & \zeta^*_{2j-1} < t \le \zeta^*_{2j}, \quad j \in \mathbb{Z}, \end{cases} \tag{13}$$

is a relay function. In (13), the sequence $\{\zeta^*_j\}$ of switching moments is generated through the equation $\zeta^*_j = j + \eta^*_j,\ j \in \mathbb{Z}$, where $\{\eta^*_j\}$ is an unpredictable trajectory of the logistic map (11).

One can confirm that $\phi(t)$ is bounded such that $\sup_{t\in\mathbb{R}} |\phi(t)| \le 3/4$. It was shown in paper [2] that the function $\phi(t)$ is the unique uniformly exponentially stable unpredictable solution of the differential equation

$$\vartheta'(t) = -2\vartheta(t) + \gamma^*(t). \tag{14}$$

It is not an easy task to visualize the unpredictable function $\phi(t)$. Therefore, in order to illustrate the chaotic dynamics, we take into account the differential equation

$$\vartheta'(t) = -2\vartheta(t) + \gamma(t), \tag{15}$$

where

$$\gamma(t) = \begin{cases} 1.5, & \zeta_{2j} < t \le \zeta_{2j+1}, \quad j \in \mathbb{Z}, \\ 0.3, & \zeta_{2j-1} < t \le \zeta_{2j}, \quad j \in \mathbb{Z}, \end{cases} \tag{16}$$

and the sequence $\{\zeta_j\}$ satisfies the equation $\zeta_j = j + \eta_j,\ j \in \mathbb{Z}$, in which $\{\eta_j\}$ is a solution of (11) with $\eta_0 = 0.4$. The coefficient 3.91 used in the logistic map (11) and the initial data $\eta_0 = 0.4$ were considered for shadowing analysis in the paper [19].

We depict in Fig. 2 the solution of Eq. 15 with $\vartheta(0) = 0.3$. It is seen in Fig. 2 that the behavior of the solution is irregular, and this support that the function $\phi(t)$ is unpredictable.

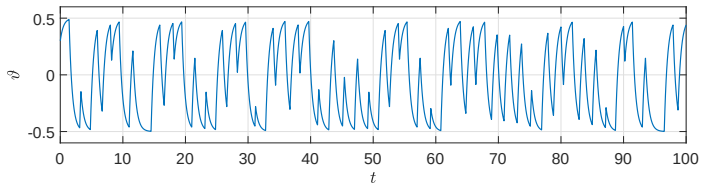

Fig. 2 The solution of Eq. 15 with $\vartheta(0) = 0.3$. The figure support that the function $\phi(t)$ is unpredictable.

2.1 Unpredictability due to the forcing source term

Let us perturb Eq. 2 with the unpredictable function $\phi(t)$ defined by (12) and set up the equation

$$\frac{\partial T}{\partial t} + u\frac{\partial T}{\partial x} + v\frac{\partial T}{\partial y} + w\frac{\partial T}{\partial z} = f(t, x, y, z, T) + \psi(\phi(t)), \tag{17}$$

where u, v, w, and f are in the form of (7) and $\psi : [-3/4, 3/4] \to \mathbb{R}$ is a continuous function.

Using the method of characteristics, one can reduce Eq. 17 to system (6) that can be expressed in the form of (10) with

$$G(X(t)) = \begin{bmatrix} U \\ V \\ W \\ F \end{bmatrix}, \qquad H(t) = \begin{bmatrix} 0 \\ 0 \\ 0 \\ \psi(\phi(t)) \end{bmatrix}.$$

According to the result of Theorem 5.2 [2], if there exist positive constants L_1 and L_2 such that

$$L_1 |s_1 - s_2| \leq |\psi(s_1) - \psi(s_2)| \leq L_2 |s_1 - s_2| \tag{18}$$

for all $s_1, s_2 \in [-3/4, 3/4]$, then the function $H(t)$ is also unpredictable.

Now, in Eq. 17, let us take $u = -0.03x + 0.1\sin(\frac{x}{80}) + 0.4$, $v = -0.01y - 0.05\sin(y)$, $w = -0.02z + (0.05\cos(y) - 0.00125\cos(\frac{x}{80}))z$, $\psi(s) = 6s$, and $f(t, x, y, z, T) = -1.5T + 0.1w_2T$. Since the conditions of Theorem 1 are valid and inequality (18) holds for these choices of ψ, f, u, v, and w, Eq. 17 exhibits Poincaré chaos.

In order to simulate the chaotic behavior, we consider the equation

$$\frac{\partial T}{\partial t} + u\frac{\partial T}{\partial x} + v\frac{\partial T}{\partial y} + w\frac{\partial T}{\partial z} = f(t, x, y, z, T) + \psi(\vartheta(t)), \tag{19}$$

where $\vartheta(t)$ is the function depicted in Fig. 2, and u, v, w, f, ψ are the same as above. Figure 3 shows the solution $T(t, x, y, z)$ of (19) corresponding to the initial condition $T(0, 0, 0, 0) = 0.5$. It is seen in Fig. 3 that the behavior of the solution is chaotic, and this supports the result of Theorem 1 such that Eq. 17 admits an unpredictable solution.

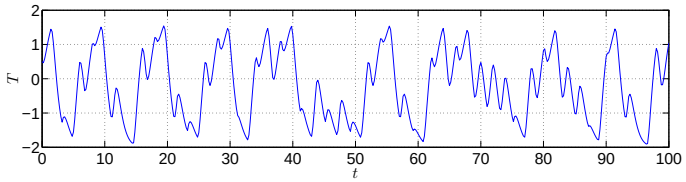

Fig. 3 The solution of Eq. 19 with the initial condition $T(0,0,0,0) = 0.5$. The figure reveals the presence of an unpredictable solution in the dynamics of (17).

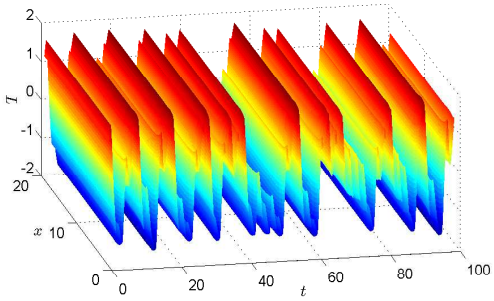

Fig. 4 The integral surface of (20). The chaotic behavior in the SST is observable in the figure.

Next, we will visualize the chaotic dynamics in the integral surface of SST. For that purpose, we omit the term of the meridional advection $v\frac{\partial T}{\partial y}$ in (17), which has less effect on SST compared with the zonal and vertical advections [10], and set up the equation

$$\frac{\partial T}{\partial t} + u\frac{\partial T}{\partial x} + w\frac{\partial T}{\partial z} = -1.5\,T + w\,T + 6\,\vartheta(t), \tag{20}$$

where $u = 1.2 + 0.1\sin(\frac{x}{80}) + 0.05\sin(3t)$ and $w = 0.1 - 0.00125\cos(\frac{x}{80})z$. In (20), $\vartheta(t)$ is again the function shown in Fig. 2.

We apply a finite difference scheme to solve Eq. 20 directly. In such a scheme, we need to specify boundary conditions along with an initial condition. Using the initial condition $T(0,x,z) = 5$ and the boundary conditions $T(t,0,z) = T(t,x,0) = 0.5$, we represent in Fig. 4 the integral surface of (20) with respect to t, x, and the fixed value $z = 0$ for $5 \le x \le 20$ and $0 \le t \le 100$. Figure 4 supports the result of Theorem 1 one more time such that Poincaré chaos is present in the dynamics.

2.2 Unpredictability due to the current velocity

This subsection is devoted to the investigation of SST when the current velocity behaves chaotically. Here, we will make use of the unpredictable function $\phi(t)$ defined by (12) to apply perturbations to the zonal and vertical components of current velocity in Eq. 2.

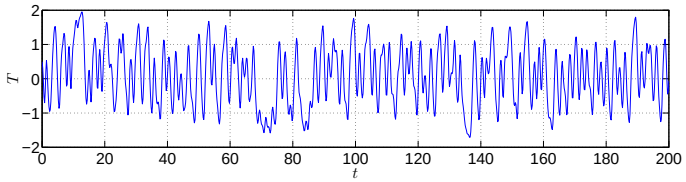

Fig. 5 The solution of (21) with $T(0,0,0,0) = 0.5$. The chaotic behavior of the solution is apparent in the figure.

We begin with considering the equation

$$\frac{\partial T}{\partial t} + [u + \psi(\phi(t))]\frac{\partial T}{\partial x} + v\frac{\partial T}{\partial y} + w\frac{\partial T}{\partial z} = f(t, x, y, z, T), \tag{21}$$

where, in a similar way to (17), u, v, w, and f are in the form of (7), and $\psi : [-3/4, 3/4] \to \mathbb{R}$ is a continuous function.

One can confirm that Theorem 1 can be used to verify the existence of Poincaré chaos in the dynamics of (21) since it can be reduced by means of the method of characteristics to a system of the form (10) with

$$H(t) = \begin{bmatrix} \psi(\phi(t)) \\ 0 \\ 0 \\ 0 \end{bmatrix},$$

which is an unpredictable function provided that ψ satisfies the condition (18).

In order to demonstrate the chaotic dynamics of (21), we take $u = -0.003\,x + 0.2\sin(\frac{x}{3}) + 0.4$, $v = -0.001\,y$, $w = -0.002\,z - \frac{0.2}{3}\cos(\frac{x}{3})\,z$, $\psi(s) = 3s$, $f = -1.5\,T - 3\sin(3x) + 0.2$, and consider the equation

$$\frac{\partial T}{\partial t} + [u + \psi(\vartheta(t))]\frac{\partial T}{\partial x} + v\frac{\partial T}{\partial y} + w\frac{\partial T}{\partial z} = f(t, x, y, z, T), \tag{22}$$

where $\vartheta(t)$ is the function shown in Fig. 2.

The time series of the solution of (22) with $T(0,0,0,0) = 0.5$ is depicted in Fig. 5. One can observe in the figure that the time series is chaotic, and this confirms the result of Theorem 1 such that Eq. 21 possesses an unpredictable solution. More precisely, the perturbation of the zonal velocity component in Eq. 2 by the unpredictable function $\psi(\phi(t))$ affects the dynamics in such a way that the perturbed Eq. 21 is Poincaré chaotic.

Next, we will examine the case when the vertical velocity component in Eq. 2 is perturbed by the unpredictable function $\phi(t)$. For this aim we set up the equation

$$\frac{\partial T}{\partial t} + u\frac{\partial T}{\partial x} + v\frac{\partial T}{\partial y} + [w + \psi(\phi(t))]\frac{\partial T}{\partial z} = f(t, x, y, z, T), \tag{23}$$

where the function $\psi : [-3/4, 3/4] \to \mathbb{R}$ is continuous. If we take $u = -0.001\,x + 0.2\sin(\frac{x}{3}) + 0.4$, $v = -0.001\,y$, $w = -0.03z - \frac{0.2}{3}\cos(\frac{x}{3})z + 3\vartheta(t)$, $\psi(s) = 3s$,

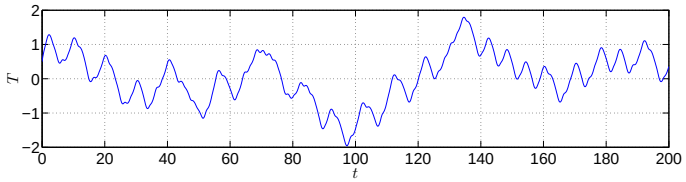

Fig. 6 Chaotic behavior of SST due to the perturbation of the vertical component of current velocity. The figure shows the solution of (24) with $T(0,0,0,0) = 0.5$.

and $f = -1.7\,T + 0.5\,z + 1.6$, then Eq. 23 admits an unpredictable solution in accordance with Theorem 1.

We represent in Fig. 6 the solution of the equation

$$\frac{\partial T}{\partial t} + u\frac{\partial T}{\partial x} + v\frac{\partial T}{\partial y} + [w + \psi(\vartheta(t))]\frac{\partial T}{\partial z} = f(t,x,y,z,T), \tag{24}$$

corresponding to the initial data $T(0,0,0,0) = 0.5$. Here, we use the same u, v, w, ψ, and f as in (23), and $\vartheta(t)$ is again the function whose time series is depicted in Fig. 2. The irregular fluctuations seen in the figure uphold the result of Theorem 1.

We end up this subsection by illustrating the influence of the chaotic current velocity on the integral surface of SST. Figure 7 (a) shows the integral surface of (21) with $u = 1.5 + 0.5\sin x$, $v = 0$, $w = 1 - 0.5\cos x$, $\psi(s) = 2s$, and $f = -1.2\,T - 3\sin(3x)$ at $z = 0$. The initial condition $T(0,x,y,z) = \sin(xz) + 1$ and the boundary conditions $T(t,0,y,z) = T(t,x,y,0) = 0.5$ are utilized in the simulation. One can see in Fig. 7 (a) that the SST has chaotic behavior in keeping with the result of Theorem 1. On the other hand, using the same initial and boundary conditions, we represent in Fig. 7 (b) the integral surface of (23) with $u = 1$, $v = 0$, $w = 1$, $\psi(s) = 2s$, and $f = -1.2\,T + 3\sin(3z)$ at $z = 1.5$. Figure 7 (b) also manifests that the applied perturbation on the vertical component of current velocity make the Eq. 23 behave chaotically even if it is initially non-chaotic in the absence of the perturbations.

3 Extension of SST Unpredictability

Chaotic behavior may transmit from one model to another [6,1]. This transmission interprets, for instance, why the unpredictability in one stock market or in the weather of one area is affected by another. Chaos in SST may be gained from another endogenous chaotic system like air temperature or wind speed. We can deal with the global ocean as a finite union of subregions. Each of these subregions may be controlled by different models depending on the position and circumstances. An assumption of the existence of chaotic and non-chaotic subregions for SST behavior is very probable. However, it seems quite unreasonable to imagine a predictable SST for one region whereas its neighbor region is characterized by an unpredictable SST. The mutual effect

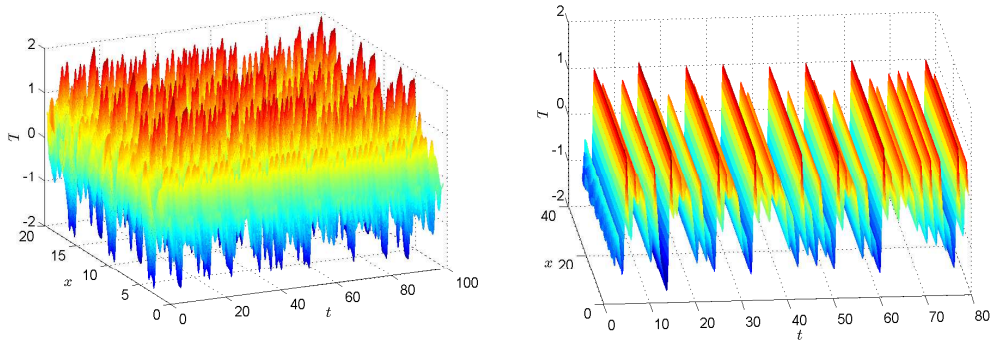

(a) The integral surface of (21) at $z = 0$

(b) The integral surface of (23) at $z = 1.5$

Fig. 7 Chaotic behavior of SST due to the current velocity with initial condition $T(0, x, y, z) = \sin(xz) + 1$, and boundary conditions $T(t, 0, y, z) = T(t, x, y, 0) = 0.5$. Both pictures in (a) and (b) reveal that chaotic behavior in the current velocity leads to the presence of chaos in SST.

in SST between neighbor regions can be seen by coupling their controlling models.

3.1 Coupling of advection equations

In this part of the paper we deal with the extension of chaos in coupled advection equations. For that purpose, we consider a Poincaré chaotic advection equation of the form (17) as the drive, and we take into account the equation

$$\frac{\partial \tilde{T}}{\partial t} + \tilde{u}\frac{\partial \tilde{T}}{\partial x} + \tilde{v}\frac{\partial \tilde{T}}{\partial y} + \tilde{w}\frac{\partial \tilde{T}}{\partial z} = \tilde{f}(t, x, y, z, \tilde{T}) + g(T) \tag{25}$$

as the response, in which g is a continuous function and T is a solution of the drive equation (17). We assume that the response does not possess chaos in the absence of the perturbation, i.e., we suppose that the advection equation

$$\frac{\partial \tilde{T}}{\partial t} + \tilde{u}\frac{\partial \tilde{T}}{\partial x} + \tilde{v}\frac{\partial \tilde{T}}{\partial y} + \tilde{w}\frac{\partial \tilde{T}}{\partial z} = \tilde{f}(t, x, y, z, \tilde{T}) \tag{26}$$

is non-chaotic.

We assume that the dynamics of the chaotic region is governed by the drive equation (17), which has an unpredictable solution, and the dynamics of the non-chaotic region is governed by Eq. 26. The coupling between these two equations leads to the transmission of unpredictability such that the response equation (25) possesses chaos.

To demonstrate the extension of chaos numerically, let us consider Eq. 25 with $u = 1.2$, $v = 0$, $w = 0.3$, $f = -1.5\tilde{T} + 0.2$, and $g(T) = T$. Using the solution T of Eq. 20 satisfying $T(0, 0, 0, 0) = 0.5$ as the perturbation in Eq. 25, we depict in Fig. 8 the solution $\tilde{T}$ of (25) corresponding to the initial

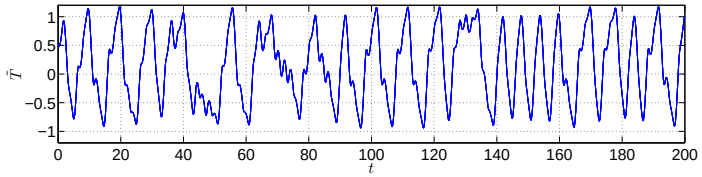

Fig. 8 The solution of the response equation (25) with initial condition $T(0,0,0,0) = 0.5$. The figure manifests the extension of chaos in the coupled system (17)-(25).

data $\tilde{T}(0,0,0,0) = 0.5$. Figure 8 reveals the extension of chaos in the coupled system (17)-(25).

3.2 Coupling of advection equation with Vallis model

The Lorenz-like form of the Vallis model is given by [37]

$$\begin{aligned} \frac{du}{dt} &= B\,T_d - C\,u, \\ \frac{dT_d}{dt} &= u\,T_s - T_d, \\ \frac{dT_s}{dt} &= -u\,T_d - T_s + 1, \end{aligned} \tag{27}$$

where u represents the zonal velocity, $T_d = (T_e - T_w)/2$, $T_s = (T_e + T_w)/2$, T_e and T_w are the SST in the eastern and western ocean respectively, and B and C are constants. It was shown in paper [37] that system (27) with the parameters $B = 102$ and $C = 3$ is chaotic. The existence of chaos in the dynamics of Vallis systems was also investigated in the studies [17,11].

Next, we take into account the equations

$$\frac{\partial T_1}{\partial t} + 1.2\frac{\partial T_1}{\partial x} + 0.3\frac{\partial T_1}{\partial z} = -1.2\,T_1 - 1 + 2\sin x, \tag{28}$$

$$\frac{\partial T_2}{\partial t} + 1.2\frac{\partial T_2}{\partial x} + 0.3\frac{\partial T_2}{\partial z} = -2\,T_2 + 4\sin x, \tag{29}$$

$$\frac{\partial T_3}{\partial t} + 0.6\frac{\partial T_3}{\partial x} + 0.5\frac{\partial T_3}{\partial z} = -2\,T_3 - 1 + 3\sin x, \tag{30}$$

and

$$\frac{\partial T_4}{\partial t} + 1.2\frac{\partial T_4}{\partial x} + 0.3\frac{\partial T_4}{\partial z} = -1.5\,T_4. \tag{31}$$

One can verify that Eqs. 28, 29, 30, and 31 are all non-chaotic such that they admit asymptotically stable regular solutions. By applying perturbations to these equations, we set up the following ones:

$$\frac{\partial T_1}{\partial t} + 1.2\frac{\partial T_1}{\partial x} + 0.3\frac{\partial T_1}{\partial z} = -1.2\,T_1 - 1 + 2\sin x + 4.6\,T_s, \tag{32}$$

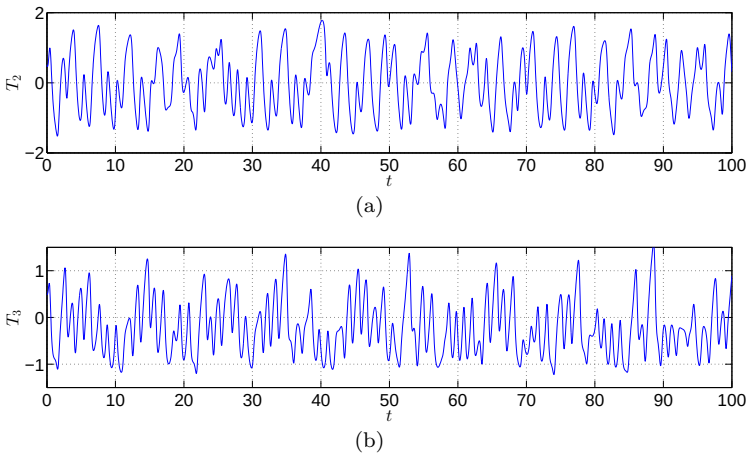

Fig. 9 The extension of the chaotic behavior by Eqs. 33 and 34. (a) The time series of the solution of Eq. 33, (b) The time series of the solution of Eq. 34. The initial data $T_2(0,0,0,0) = 0.5$ and $T_3(0,0,0,0) = 0.5$ are used.

$$\frac{\partial T_2}{\partial t} + (1.2 + 0.8\,u)\frac{\partial T_2}{\partial x} + 0.3\frac{\partial T_2}{\partial z} = -2\,T_2 + 4\sin x, \tag{33}$$

$$\frac{\partial T_3}{\partial t} + (0.6 + u)\frac{\partial T_3}{\partial x} + 0.5\frac{\partial T_3}{\partial z} = -2\,T_3 - 1 + 3\sin x + 4\,T_s, \tag{34}$$

$$\frac{\partial T_4}{\partial t} + 1.2\frac{\partial T_4}{\partial x} + 0.3\frac{\partial T_4}{\partial z} = -1.5\,T_4 + 2.7\,T_2, \tag{35}$$

where (u, T_d, T_s) is the solution of the chaotic Vallis model (27) with $B = 102$ and $C = 3$ corresponding to the initial conditions $u(0) = 2$, $T_d(0) = 0.2$, and $T_s(0) = 0.4$.

In Eq. 32 the forcing term is perturbed by the SST average, T_s, whereas in Eq. 33 the zonal velocity of Vallis model, u, is used as perturbation. On the other hand, in Eq. 34 both the forcing term and the zonal velocity components are perturbed with the solution of (27). Moreover, the solution T_2 of (33) is used as a perturbation in the forcing term of Eq. 35. The appearance of the zonal velocity u of the model (27) in the coefficients of Eqs. 33 and 34 looks reasonable if one remembers that the parts of the ocean surface under consideration are adjoining to each other, and consequently, the zonal velocity u perturbs its counterpart in the neighbor region from 1.2 to $1.2 + 0.8u$ in Eq. 33 and from 0.6 to $0.6 + u$ in Eq. 34. Furthermore, the perturbations with T_s in Eqs. 32 and 34 can be attributed to the heat transfer between the neighbor regions because of the structure of the original equation (2).

Figure 9 (a) and (b) respectively show the solutions T_2 of Eq. 33 and T_3 of Eq. 34. The initial data $T_2(0,0,0,0) = 0.5$ and $T_3(0,0,0,0) = 0.5$ are used in the simulations. Figure 9 reveals that the chaos of the model (27) is extended by Eqs. 33 and 34.

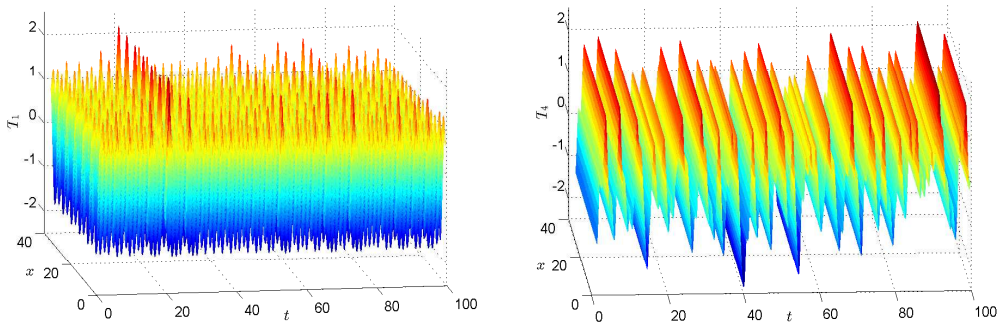

(a) (b)

Fig. 10 Extension of chaos by Eqs. 32 and 35. (a) The integral surface of Eq. 32, (b) The integral surface of Eq. 35.

On the other hand, we depict in Fig. 10 (a) and (b) the 3-dimensional integral surfaces corresponding to the solutions T_1 of Eq. 32 and T_4 of Eq. 35, respectively. Here, we make use of the boundary conditions $T_1(0,x,z) = T_1(t,0,z) = T_1(t,x,0) = 0.5$ and $T_4(0,x,z) = T_4(t,0,z) = T_4(t,x,0) = 0.5$. The figure confirms one more time that the chaos of system (27) is extended.

3.3 Coupling of Vallis models

Our purpose in this subsection is to demonstrate numerically our suggestion that chaos can be extended between the regions of some global climate variabilities. We assume that there are intermediate subregions located between these main regions and chaos can transmit from one region to another in a sequential way.

We also suggest that the IOD can be described by a Vallis model in the form of (27) with parameters appropriate to the Indian Ocean. Evaluation of these parameters is rather difficult. However, for simplicity we can choose these values such that system (27) does not exhibit chaotic behavior.

To demonstrate the extension of chaos, let us consider the perturbed Vallis system

$$\begin{aligned}
\frac{d\tilde{u}}{dt} &= \tilde{B}\,\tilde{T}_d - \tilde{C}\,\tilde{u} + 1.5\,u,\\
\frac{d\tilde{T}_d}{dt} &= \tilde{u}\,\tilde{T}_s - \tilde{T}_d + 0.3\,T_d,\\
\frac{d\tilde{T}_s}{dt} &= -\tilde{u}\,\tilde{T}_d - \tilde{T}_s + 1 + 0.2\,T_s,
\end{aligned} \tag{36}$$

where (u, T_d, T_s) is the solution of the chaotic Vallis system (27) with $B = 102$ and $C = 3$ corresponding to the initial conditions $u(0) = 2$, $T_d(0) = 0.2$ and

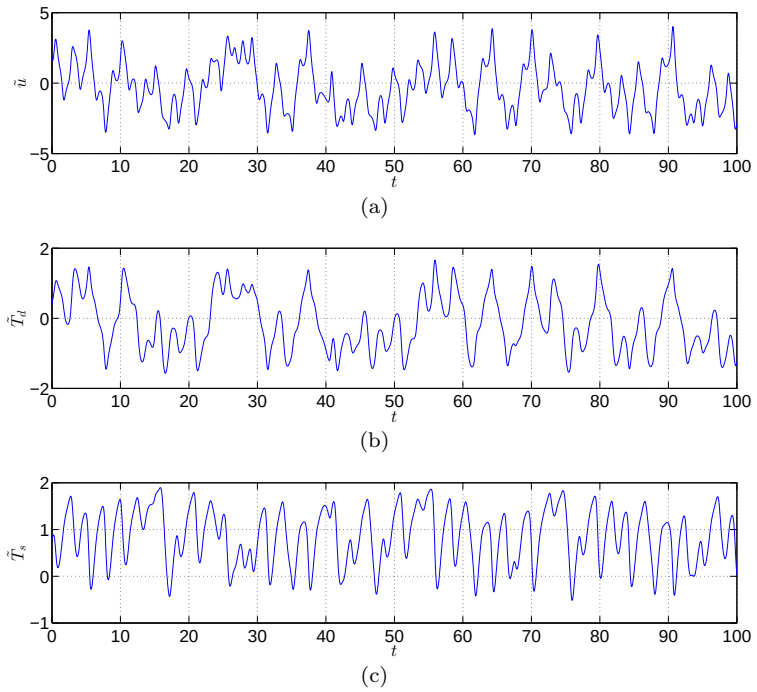

Fig. 11 The solution of system (36). The figure reveals chaos extension between the pair of Vallis systems (27) and (36)

$T_s(0) = 0.4$. We use the parameters $\tilde{B} = 20$ and $\tilde{C} = 7$ in (36) and assume that the unperturbed Vallis model

$$\begin{aligned} \frac{d\tilde{u}}{dt} &= \tilde{B}\,\tilde{T}_d - \tilde{C}\,\tilde{u}, \\ \frac{d\tilde{T}_d}{dt} &= \tilde{u}\,\tilde{T}_s - \tilde{T}_d, \\ \frac{d\tilde{T}_s}{dt} &= -\tilde{u}\,\tilde{T}_d - \tilde{T}_s + 1, \end{aligned} \tag{37}$$

represents the IOD with these parameter values. Utilizing the initial conditions $\tilde{u}(0) = 2$, $\tilde{T}_d(0) = 0.2$, and $\tilde{T}_s(0) = 0.4$, we represent in Fig. 11 the time series of $\tilde{u}$, $\tilde{T}_d$, and $\tilde{T}_s$ coordinates of the solution of system (36). One can see in Fig. 11 that system (36) possesses chaotic behavior.

4 Conclusion

In this paper we discuss the possible unpredictable behavior of hydrosphere variables. ENSO variability is suggested to be chaotic by many studies. The well-known Vallis ENSO chaotic model is one among several ENSO models

that exhibit irregular behavior. The presence of chaos in ENSO can be indicated by the behavior of SST as well as ocean current velocity. We describe the dynamics of SST by the advection equation. The forcing term, based on ocean-atmosphere interaction, and the current velocity in this equation can be a source of unpredictability in SST. We prove the presence of chaos in SST dynamics by utilizing the concept of unpredictable function. The relationship and interaction between the climate variabilities, like the ones between ENSO and IOD, have attracted attention in recent literature. Constructing and understanding the dynamic models driving these phenomena are the main steps to investigate the mutual influences between these global events. The SST anomalies are closely linked to some climate variabilities teleconnections in different parts of the global ocean. We suggest that the hydrosphere characteristics can behave chaotically through the possibility of transmission of chaos between ocean neighbor subregions. We verified this transmission by different "toy" couples of advection equations and Vallis models. The simulations of these couples show that unpredictability can be transmitted from a local region controlled by a chaotic model into its neighbor which is described by a non-chaotic model. Further investigation can done by including different models for more climate components.

References

1. Akhmet, M. and Fen, M. O., Extension of Lorenz unpredictability, Int. J. Bifurcat. Chaos, 25, 10, 1550126 (2015).
2. Akhmet, M. and Fen, M. O., Poincar chaos and unpredictable functions, Commun. Nonlinear Sci. Numer. Simulat., 48, 85-94 (2017).
3. Akhmet, M. and Fen, M. O., Unpredictable points and chaos, Commun. Nonlinear Sci. Numer. Simulat., 40, 1-5 (2016).
4. Akhmet, M. and Fen, M. O., Existence of unpredictable solutions and chaos, Turk. J. Math., 41, 254-266 (2017).
5. Akhmet, M. and Fen, M. O., Non-autonomous equations with unpredictable solutions, Commun. Nonlinear Sci. Numer. Simulat., 59, 657-670 (2018).
6. Akhmet, M. U. and Fen, M. O., Replication of chaos, Commun. Nonlinear Sci. Numer. Simulat., 18, 2626-2666 (2013).
7. Barale, V. and Gade, M., Remote Sensing of the European Seas, Springer Science Business Media, B.V. (2008).
8. Battisti, D. S., Dynamics and thermodynamics of a warming event in a coupled tropical atmosphereocean model, J. Atmos. Sci., 45, 2889-2919 (1988).
9. Behera, S. K., Luo, J. J., Masson, S., Rao, S. A., Sakuma, H. and Yamagata, T., A CGCM study on the interaction between IOD and ENSO, J. Climate, 19, 1688-1705 (2006).
10. Bonjean, F., Influence of sea currents on the sea surface temperature in the tropical Pacific ocean, J. Phys. Oceanogr., 31, 943-961 (2001).
11. Borghezan, M. and Rech, P. C., Chaos and periodicity in Vallis model for El Nio, Chaos Soliton. Fract., 97, 15-18 (2017).
12. Chambers, D. P., Tapley, B. D. and Stewart, R. H., Anomalous warming in the Indian Ocean coincident with El Nio, J. Geophys. Res., 104, 3035-3047 (1999).
13. Coley, D., Energy and Climate Change: Creating a Sustainable Future, John Wiley and Sons, Chichester. UK (2008).
14. Devaney, R. L., An Introduction to Chaotic Dynamical Systems, Addison-Wesley, Menlo Park (1989).
15. Eamus, D., Huete, A. and Yu, Q., Vegetation Dynamics: A Synthesis of Plant Ecophysiology, Remote Sensing and Modelling, Cambridge University Pressg, New York (2016).

16. Feigenbaum, M. J., Universal behavior in nonlinear systems, Los Alamos Sci./Summer., 1, 4-27 (1980).
17. Garay, B. M. and Indig, B., Chaos in Vallis' asymmetric Lorenz model for El Nio, Chaos Soliton. Fract., 75, 253-262 (2015).
18. Gent, P. R. and Cane, M. A., A reduced gravity, primitive equation model of the upper equatorial ocean, J. Comput. Phys., 81, 444-480 (1989).
19. Hammel, S. M., Yorke, J. A. and Grebogi, C., Do numerical orbits of chaotic dynamical processes represent true orbits, J. Complexity, 3, 136-145 (1987).
20. Jochum, M. and Murtugudde, R., Temperature advection by tropical instability waves, J. Phys. Oceanogr., 36, 592-605 (2006).
21. Kessler, W. S., Rothstein, L. M. and Chen, D., The annual cycle of SST in the eastern tropical Pacific as diagnosed in an OGCM, J. Climate, 11, 777-799 (1998).
22. Li, T. Y. and Yorke, J. A., Period Three Implies Chaos, Amer. Math. Monthly, 82, 985-992 (1975).
23. Lucas, L. E., Waliser, D. E. and Murtugudde, R., Mechanisms governing sea surface temperature anomalies in the eastern tropical Pacific Ocean associated with the boreal winter Madden-Julian Oscillation, JGR-Oceans, 115, C05012 (2010).
24. Lukas, R. and Lindstrom, E., The mixed layer of the western equatorial Pacific ocean, J. Geophys. Res., 96, 3343-3357 (1991).
25. Luo, J. J., Zhang, R. C., Behera, S. K., Masumoto, Y., Jin, F. F., Lukas, R. and Yamagata, T., Interaction between El Nio and extreme Indian Ocean Dipole, J. Climate, 23, 726-742 (2010).
26. Münnich, M., Cane, M. A. and Zebiak, S. E., A study of self-excited oscillations in a tropical oceanatmosphere system, Part II: Nonlinear cases, J. Atmos. Sci., 48, 1238-1248 (1991).
27. Neelin, J. D. and Latif, M., El Nio dynamics, Phys. Today, 51, 12, 32-36 (1998).
28. Penland, C. and Matrasova, L., A balance condition for stochastic numerical models with application to the El Nio-Southern Oscillationl, J. Climate, 7, 1352-1372 (1994).
29. Roxy, M., Guladi, S., Drobhlar, H. K. L. and Navarra, A., Seasonality in the relationship between El Nio and Indian Ocean Dipole, Clim. Dyn., 37, 221236 (2011).
30. Saji, N. H., Goswami, B. N., Vinayachandran, P. N. and Yamagata, T., A dipole mode in the tropical Indian ocean, Nature, 401, 360-362 (1999).
31. Sander, E. and Yorke, J. A., Period-doubling cascades galore, Ergod. Theory Dyn. Syst., 31, 1249-1267 (2011).
32. Schöll, E. and Schuster, H. G.(Eds.), Handbook of Chaos Control, WileyVCH, Weinheim. Germany (2008).
33. Sell, G. R., Topological Dynamics and Ordinary Differential Equations, Nostrand-Reinhold, London (1971).
34. Stevenson, J. W. and Niiler, P. P., Upper ocean heat budget during the Hawaii-to-Tahiti Shuttle Experiment, J. Phys. Oceanogr., 13, 1894-1907 (1983).
35. Stuecker, M. F., Jin, F. F. and Timmermann, A., El Nio-Southern Oscillation frequency cascade, Proc. Natl. Acad. Sci. U.S.A., 112, 13490-13495 (2015).
36. Tziperman, E., Stone, L., Cane, M. A. and Jarosh, H., El Nio chaos: Overlapping of resonance between the seasonal cycle and the Pacific ocean-atmosphere oscillator, Science, 264, 72-74 (1994).
37. Vallis, G. K., Conceptual models of El Nio and the Southern Oscillation, J. Geophys., 93, 13979-13991 (1988).
38. Willebrand, J. and Anderson, D. L. T.(Eds.), Modelling Oceanic Climate Interactions, Springer-Verlag, Berlin Heidelberg (1993).
39. Yamagata, T., Behera, S. K., Luo, J. J., Masson, S., Jury, M. R. and Rao, S. A., Coupled oceanatmosphere variability in the tropical Indian ocean, Earth's climate: The oceanatmosphere interaction, Geophys. Monogr., 147, 189-212 (2004).
40. Zebiak, S. E. and Cane, M. A., A model El Nio-Southern Oscillation, Mon. Wea. Rev., 115, 2262-2278 (1987).